

# On Earthquake Ground Motion and Structural Response in Alluvial Valleys

By Jacobo Bielak<sup>1</sup>, Member ASCE, Jifeng Xu<sup>2</sup>,  
and Omar Ghattas<sup>3</sup>

**ABSTRACT:** This paper is concerned with the problem of soil amplification and structural damage due to local site conditions in sedimentary valleys during earthquakes. It focuses on a small valley in Kirovakan, for which one dimensional (1D) wave propagation analyses have failed to provide adequate answers for the large extent and spatial distribution of damage during the 1988 Armenia Earthquake. A more realistic two-dimensional finite element analysis is performed herein in search of an explanation for the observed behavior. Using as input an inferred rock accelerogram, the response of the valley is calculated for a vertically incident SH-wave. Synthetic accelerograms of the surface ground motion are presented for different sites; these accelerograms are then used to determine the amplification ratios of the surface response with respect to that of the free-field motion of the rock outcrop, for different frequencies and for a continuous set of sites. In addition, response spectra are evaluated for simple oscillators representing structures located at various sites. Results of the 2D simulations show striking differences with respect to those from 1D analyses. In particular, (a) while the resonant frequencies exhibited by a 1D model for a given site also appear in the 2D model, the peak ground response and structural response are almost twice as large for the 2D as for the 1D model; (b) the 2D model exhibits, in addition, a new set of resonant frequencies and concomitant “mode shapes” across the valley, which are directly related to its finite width; (c) due to these additional resonances the ground amplification ratio tends to oscillate very rapidly, both spatially and with frequency, leading to the observation that two identical structures located in the same vicinity or two slightly different structures located essentially on the same site can be subjected to significantly different seismic forces, even if the underlying soils have very similar characteristics. These results provide a meaningful explanation for the observed damage, and thus, serve to exemplify a situation in which site effects caused by the finite lateral extent of a valley must be taken into consideration in order to model satisfactorily seismic behavior.

---

<sup>1</sup>Professor and Director, Computational Mechanics Laboratory, Department of Civil and Environmental Engineering, Carnegie Mellon University, Pittsburgh, PA 15213

<sup>2</sup>Research Assistant, Computational Mechanics Laboratory, Department of Civil and Environmental Engineering, Carnegie Mellon University, Pittsburgh, PA 15213.

<sup>3</sup>Associate Professor and Co-Director, Computational Mechanics Laboratory, Department of Civil and Environmental Engineering, Carnegie Mellon University, Pittsburgh, PA 15213

## INTRODUCTION

The 7 December 1988, magnitude  $M_s$  6.8, earthquake in northern Armenia caused unprecedented destruction and fatalities within the epicentral region for an earthquake of this size. A number of studies have shed considerable light on the seismological, geological, geotechnical, and structural aspects of this earthquake (e.g., Wyllie and Filson 1989; Borchardt, 1989; Bommer and Ambraseys, 1989; Cisternas *et al*, 1989; Hadjian, 1993; Yegian *et al*, 1994a, 1994b, 1994c, 1994d). Of particular interest to the present study are the papers by Yegian *et al*, which contain highly useful information on the statistics of damage in several affected cities, correlated to geologic and soil profiles, and an analytical investigation of the possible role of the local soil conditions on the extent and distribution of damage to structures. Yegian, Ghahraman, and Gazetas performed one-dimensional (1D) wave-propagation analyses, using soil profiles with field and laboratory measured parameters, to explain the damage statistics in various zones of Leninakan (Yegian *et al*, 1994c) and Kirovakan (Yegian *et al*, 1994d), two cities located near the fault. These 1D simulations, based on the usual assumption of flat horizontal layers, provided adequate answers for zones in which the underlying soils consist of shallow (less than 30 m) dense gravelly sands and stiff clays, or for valleys with large width-to-depth ratios. However, by comparing the results of the 1D analyses with observed damage, they found that such analyses substantially underpredicted the ground surface motion in one region in Kirovakan in which the soil profile constitutes a triangular sedimentary basin whose width is only about five times its depth.

The main objective of the present study is to investigate whether an alternative, more realistic, model of this valley can produce a closer agreement between the results of earthquake simulations of the soil and structural response and the observed damage. Kirovakan provides a particularly appropriate case study for two reasons: (1) the available soil profiles with field and laboratory measured parameters for its various zones allow one to construct realistic mathematical models, and (2) the summaries of the respective building-damage statistics make it possible to compare the simulated behavior of structures against their actual performance.

Kirovakan has been subdivided by Yegian *et al* (1994d) into five zones to describe the great variations that exist in the subsurface soil conditions within that city. Our study will focus on one small region comprised of soils from two adjacent zones, as shown on the geotechnical profile of Fig. 1. The soil profile in Zone 3 consists of up to 30 m of stiff cohesionless alluvium of silty gravel with sands and pebbles, underlain by dense sand and gravel with pebbles and boulders. Zone 2 is filled with a thin layer of medium-stiff clays on top of stiffer clays down to about 150 m. The width-to-maximum thickness ratio of the alluvium basin of Zone 3 and the clay basin of Zone 2 is about 15 and 5, respectively. Damage statistics within the two zones are also shown on Fig. 1. These statistics indicate that damage in Zone 2 was very severe and much greater than in Zone 3.

Thus, whereas nearly three fourths of the buildings in Zone 2 collapsed or were damaged beyond repair, only five percent of the buildings within Zone 3 were damaged heavily, and more than half experienced minor or no damage. Also, all the buildings that collapsed during the earthquake were located in Zone 2. That is a very impressive contrast within a basin whose lateral extent is less than 2 km.

Yegian *et al* (1994d) attributed the unusually high damage in Zone 2 to 3D valley effects and used a simple analysis limited to a homogeneous deposit to explain this behavior. As a first step toward gaining a better physical understanding of the differences in the earthquake response of one-dimensional and multi-dimensional models of the small valley in Kirovakan depicted in Fig. 1, in this paper we consider a layered, damped, two-dimensional, linearly elastic model subjected to a transient incident plane SH-wave with a time signal derived from an actual record obtained during the 1988 Armenia Earthquake within the epicentral region. SH-waves are selected as they represent the simplest case of waves propagating in an elastic medium; their effect, however, is similar to that of more complicated situations (Bard and Bouchon, 1985). While the response within Zone 2 can be expected to enter into the inelastic range for a sufficiently strong excitation, elastic analyses such as the one reported here provide a useful reference point.

Attention is given herein to: (1) evaluating and interpreting the seismic ground motion of Zones 2 and 3 in Kirovakan, as determined from simulations from the two-dimensional model; (2) comparing the results with those from corresponding 1D models; (3) determining response spectra for the various 1D and 2D synthetic accelerograms; and (4) relating the results of the simulations to the observed damage. We illustrate not only the overall stronger ground motion in Zone 2 with respect to that in Zone 3 but also a drastic spatial variation of ground motion within Zone 2 itself and the corresponding structural response for structures with different fundamental natural frequencies. A comparison of results between Kirovakan and Leninakan is also included in this paper. This comparison is of particular interest because while the response spectra for 1D simulations in Leninakan and in Zone 2 in Kirovakan are quite similar, the corresponding levels of damage are very different.

Two-dimensional models have been used extensively over the last 25 years for investigating the effects of lateral confinement of valleys on seismic ground motion (see, e.g., Aki and Larner, 1970; Boore *et al*, 1971; Trifunac, 1971; Sánchez-Sesma and Esquivel, 1979; Bard and Bouchon, 1980a, 1980b; Vidale and Helmberger, 1988 for representative papers, and Aki, 1988, 1993, for state-of-the-art surveys). These studies have demonstrated that a curved basin bottom and body-wave to surface-wave conversion at the valley edges can have a profound effect on the surface ground motion, by prolonging the duration of shaking or by increasing the amplitude of motion. Recent observations (e.g., Spudich and Iida, 1993; Hartzell *et al*, 1996) have underscored the need for doing

2D and even 3D simulations in order to capture correctly these effects.

Several methods have been used to analyze the seismic response of basins. Analytical techniques can be applied only for simple geometries and uniform deposits that allow separation of variables of the governing equations (e.g., Trifunac, 1971; Wong and Trifunac, 1974; Sánchez-Sesma, 1983; Lee, 1990). For models of realistic basins with irregular shapes and heterogeneous materials, numerical procedures become essential. The most widely used include the finite difference method (e.g., Alterman and Karal, 1968 and Boore, 1972 in 2D, and Frankel, 1993 in 3D), the finite element method (e.g., Lysmer and Drake, 1971; Smith, 1975; Li *et al*, 1992; Toshinawa and Ohmachi, 1992; Bao *et al*, 1996), the boundary element method (e.g., Bouchon and Aki, 1977; Sánchez-Sesma, 1983; Bard and Bouchon, 1985; Kawase, 1988; Sánchez-Sesma *et al*, 1993), and combinations of the latter two (e.g., Mossessian and Dravinski, 1987; Bielak *et al*, 1991). The finite difference and finite element methods can deal effectively with geometrically complex basins with highly heterogeneous materials. They require, however, that the original problem, which involves the basin and its surrounding semi-infinite domain, be truncated by the introduction of an artificial boundary on which one must specify an approximate radiation condition to limit spurious wave reflections. They also require that the governing differential equations be solved over the entire computational domain. Upon discretization one obtains a large, yet sparse, system of algebraic equations. The boundary element method, by contrast, is based on a boundary integral formulation of the problem. Its main attributes are that the radiation conditions are satisfied automatically and that only the boundary of the basin need be considered if the valley consists of horizontal, homogeneous layers. While the number of algebraic equations obtained upon discretization is much smaller than that for the finite difference or the finite element method, the resulting system is dense. Also, if the material in the basin is highly heterogeneous, the application of the boundary element method becomes cumbersome. In this paper, we use a 2D version of a parallel elastic wave propagation finite element simulation code developed as an intermediate step towards a more general, 3D, finite element code for modelling of earthquake ground motion in large sedimentary basins on parallel computers (Bao *et al*, 1996). We favor finite elements for their ability to efficiently resolve multi-scale phenomena and the ease with which they handle traction interface and boundary conditions.

## **ANALYSIS OF THE VALLEY**

### **Description of model**

The valley model under investigation (Fig. 2) represents an idealization of the geotechnical profile in Kirovakan depicted in Fig. 1. It consists of two distinct isotropic, linearly elastic subvalleys underlain by a basement rock that extends to infinity; like the actual profile, the two subvalleys are separated by a slant edge. The two subvalleys are denoted, as in Fig. 1, as Zones 2 and 3, and are

subdivided, respectively, into 4 and 2 homogeneous layers. The corresponding depths, shear wave velocities,  $V_s$ , densities,  $\rho$ , and damping ratios,  $\zeta$ , are also given in Fig. 2, next to a soil column representative of each zone. The values of the shear wave velocity and density are based on Yegian *et al* (1994d), while those for the damping ratio are representative of the corresponding soils. The deposits in Zone 2 are significantly softer than those in Zone 3; the impedance ratio (ratio of the products of density and shear wave velocity) between the basement rock and the top layer in each zone is 7.1 and 1.9, respectively. In addition, Zone 2 is deep and narrow while Zone 3 is shallow and long. The large impedance ratio and the small width-to-depth ratio in Zone 2 foreshadow the strong effect that the surface waves generated at the confluence of the valley surface with the surrounding rock have on the valley response.

### Method of analysis

The mathematical problem under consideration is one of earthquake-induced waves traveling from a homogeneous halfspace of rock into a basin with heterogeneous soils and irregular geometries. To completely specify the problem, consider first a halfspace made up of the basement rock material. Suppose there is a transient incident plane SH-wave that produces an incident plus reflected displacement field  $u_o$ , which is a function of position and time, and is polarized perpendicularly to the cross-sectional plane of the valley. This is the free-field displacement. Suppose now that the valley, idealized as an infinitely long cylinder with an irregular cross section, is inserted in the free surface, as shown in Fig. 2. The problem, then, is to determine the total displacement (antiplane) field,  $u$ , within and outside the valley due to the incident field.

Since the soil material is assumed to be piecewise uniform,  $u$  satisfies the wave equation

$$\frac{\partial^2 u}{\partial t^2} = V_s^2 \nabla^2 u \quad (1)$$

in each subdomain and in the exterior region occupied by the rock. The displacement  $u$  and the traction are required to be continuous across each subdomain, and the traction must vanish at the free surface. The system is initially at rest.

To solve this problem, we will use the finite element method with a mesh tailored to the local wavelength of the propagating waves. Two important issues must be considered for solving wave propagation problems in infinite domains by this method. One, mentioned already in the Introduction, is the need to render the domain of computation finite and to limit the occurrence of spurious reflections. This is accomplished here by introducing the outermost circular segment I-I shown in Fig. 3a as an artificial boundary. On this arc we impose an absorbing boundary condition that is local in both space and time (Bayliss and Turkel, 1980). We use the implementation procedure proposed by Kallivokas *et al* (1991), which produces symmetric element damping and stiffness ma-

trices. These can be readily incorporated into standard finite element software. Physically, this boundary condition can be interpreted as a set of springs and dashpots distributed along the arc.

The second point that requires attention is the need to incorporate the excitation into the model when the earthquake source is located outside the computational domain. This is carried out by means of a method developed by Bielak and Christiano (1984) and Cremonini *et al* (1988) that expresses the earthquake excitation in the form of applied nodal forces acting on a strip of finite elements located outside the region of interest. The interface between the two regions is chosen as the circular arc II-II. The basic idea is straightforward. One introduces a new variable  $w$  which in the region interior to II-II coincides with the total displacement field  $u$  and on the exterior is equal to the scattered field  $u - u_o$ . Since  $u_o$  is a solution of the wave equation over the entire halfspace, then  $w$  is also governed by Eq. 1 in each subdomain. To ensure that the solution for  $w$  is equivalent to that of the original problem, continuity of the total displacement  $u$  and the corresponding traction must be imposed across II-II. When expressed in terms of  $w$ , these conditions introduce the free-field displacement  $u_o$  and the corresponding traction on II-II explicitly into the formulation. It is these terms that upon discretization give rise to the equivalent nodal forces on exterior elements containing nodes on II-II. Besides yielding the equivalent seismic forces, which are exact within discretization error, another advantage of formulating the problem in terms of the variable  $w$  is that the motion exterior to II-II will be purely outgoing. The absorbing boundary I-I need then transmit only outgoing waves.

The reduced problem defined over the bounded domain shown on Fig. 3a is solved with a 2D version of the parallel elastic finite element wave propagation code mentioned in the preceding section. The components of the system include a 2D and a 3D mesh generator, a mesh partitioner, a parceler, and a parallel code generator, as well as parallel numerical methods for applying the seismic forces, incorporating the absorbing boundaries, and solving the discretized wave propagation problem (Bao *et al*, 1996). The finite element mesh, shown in Fig. 3b, is generated by Triangle, a 2D quality mesh generator (Shewchuk, 1996). Triangle operates on geometric boundaries and interfaces defined by piecewise straight segments, as illustrated in Fig. 3a. The length of each segment is chosen according to the local material properties and maximum frequency of interest, so that Triangle produces a well-tailored unstructured mesh, as shown in Fig. 3b. Even though this problem is small and can be solved on a single processor, the simulations were performed on 64 processing elements of an Intel Paragon and a Cray T3D as a test of the parallel implementation. The corresponding partitioned mesh is presented in Fig. 3c. Each subdomain is mapped onto a processor of the parallel machine.

Quadratic six-node subparametric elements and standard Galerkin ideas are used for the spatial discretization of the governing wave equation over the triangular mesh in Fig. 3b. This leads to a

system of ordinary differential equations of the form:

$$\mathbf{M}\ddot{\mathbf{w}} + \mathbf{C}\dot{\mathbf{w}} + \mathbf{K}\mathbf{w} = \mathbf{f}(t) \quad (2)$$

in which  $\mathbf{w}$  is the vector of time-dependent nodal displacements, an overdot denotes differentiation with respect to time,  $\mathbf{M}$ ,  $\mathbf{C}$ , and  $\mathbf{K}$  are the global mass, damping, and stiffness matrices, and  $\mathbf{f}$  is the vector of equivalent nodal forces. The stiffness and damping matrices  $\mathbf{K}$  and  $\mathbf{C}$  contain terms representing the stiffness and material damping in the soil as well as those arising from the absorbing boundary condition. Damping in the soil is assumed to be of the Rayleigh type, that is, within each finite element the damping matrix is of the form:

$$\mathbf{C}^e = \alpha \omega_o \mathbf{M}^e + \frac{\beta}{\omega_o} \mathbf{K}^e \quad (3)$$

in which  $\alpha$  and  $\beta$  are arbitrary scalars,  $\omega_o$  is a reference frequency, and  $\mathbf{M}^e$  and  $\mathbf{K}^e$  are the element mass and stiffness matrices. With this choice of damping, the mass proportional and stiffness proportional terms in Eq. 2 yield a damping ratio that is inversely and directly proportional to frequency, respectively. Since the damping ratio in soils is usually assumed to remain constant independently of the rate of application of the load, Rayleigh damping can represent this behavior only approximately. This approximation is achieved here by evaluating  $\alpha$  and  $\beta$  for each soil material such that the squared difference between the target damping ratio within each soil and the actual damping ratio specified over a prescribed frequency range of interest  $[\omega_b, \omega_f]$  is minimized; that is

$$\min_{\alpha, \beta} \int_{\omega_b}^{\omega_f} \left[ \zeta - \left( \frac{\alpha \omega_o}{2 \omega} + \frac{\beta \omega}{2 \omega_o} \right) \right]^2 d\omega \quad (4)$$

The range  $[\omega_b, \omega_f]$  is selected so as to include the dominant frequencies of the earthquake excitation and the dominant resonant frequencies of the valley. The same approach can be used if  $\zeta$  is frequency-dependent.

After assembly of the individual mass, damping, and stiffness matrices, and of the equivalent seismic forces, Eq. 2 is solved numerically by the unconditionally stable Newmark's trapezoidal step-by-step method. An iterative method, Jacobi preconditioned conjugate gradients, is used to solve the resulting algebraic equations at each time step, as this is more efficient than a direct solver on a parallel computer.

It is important to emphasize that while Eq. 2 provides an approximate solution for the total displacement field within the valley and the surrounding region due to an arbitrary incident SH-wave generated outside the computational domain, this equation strictly characterizes the response of a bounded domain. Since  $\mathbf{M}$  and  $\mathbf{K}$  are symmetric and positive definite, it then follows that the reduced system that governs the undamped free vibrations of the elastically supported valley, which is obtained from Eq. 2 by setting to zero the damping and forcing terms, possesses

undamped natural frequencies and corresponding orthogonal modes. For the damped case these modes are not classical, in general, due both to the type of soil damping considered and to the contribution to  $\mathbf{C}$  from the absorbing boundary condition. However, the damped system has complex conjugate eigenvalues and associated complex conjugate orthogonal eigenvectors (Foss, 1958). The eigenvalues represent damped natural frequencies and exponential attenuation. The response to a prescribed excitation, including the incident seismic wave, can be expressed as a linear combination of the individual modes. The extent to which each individual complex conjugate eigenvector pair of the valley model (mode shapes) contributes to the total response depends, of course, on the particular spatial and temporal distribution of the seismic excitation.

## **SIMULATION OF ARMENIA EARTHQUAKE**

### **Ground motion**

Only one set of good-quality strong-motion records was obtained of the main shock of the 1988 Armenia Earthquake, in the town of Ghoukasian about 30 km northwest of the epicenter, in a station located on the ground surface. This town is built on top of an extended shallow deposit of alluvium and lake-bed clay layers underlain by rock. In order to obtain a reference motion for this region, Yegian *et al* (1994a) performed a 1D wave propagation analysis to remove the soil amplification effects. This resulted in rock outcrop acceleration histories with a maximum value of 0.25 g in the horizontal direction. To estimate the corresponding peak ground acceleration (PGA) in Kirovakan, they used observations of grave markers in cemeteries in that city, along with subsequent shaking table tests on model blocks, and found that this PGA did not exceed 0.15 g. They then scaled the reference rock outcrop motion to 0.15 g and used the scaled records to perform 1D analyses of the soil amplification in Kirovakan. The N-S component of the scaled reference acceleration is shown on Fig. 4. This accelerogram, scaled here by one half to account for the doubling of the amplitude as the incident SH-wave reaches the free surface of the halfspace, will be the excitation considered in our simulations. Also, following common practice in geotechnical engineering amplification studies, the incident, plane SH-wave will be assumed to propagate vertically through the halfspace. The resulting response of the valley model (Fig. 2) will consist of SH- and surface (Love) waves. Results of the simulations will be presented both in the time domain and in the frequency domain. To assist in their interpretation, the amplitude of the Fourier transform of the acceleration trace is also included in Fig. 4. Notice that the frequency content of the reference acceleration is most significant in the vicinity of 2.5 Hz. The relevance of this observation will become apparent in the next section.

### **Numerical results**

In this section, we describe several different representations of the results of the 2D ground



motion simulation, and compare the results with those from corresponding 1D models. We also introduce a simple rectangular valley to assist in the interpretation of the results, and calculate response spectra of simple structures located at different sites within the Kirovakan model in order to relate the simulated performance to the observed damage. In addition, a response spectrum is calculated for the city of Leninakan, as a means for explaining differences in the observed structural performance between the two cities.

Synthetic accelerograms for several points along the free surface of the valley and its vicinity are shown in Fig. 5a. The locations of these points are identified by the labels A to I in Fig. 2. For points outside the valley the motion differs little from the free-field motion. Inside the valley, however, the response is amplified significantly, especially in Zone 2. This can further be seen in Fig. 5b, in which the PGA along the entire valley surface is graphed as a solid line. In Zone 3, the average amplification with respect to the free-field value is about 30 percent, with a slight increase toward the right edge, which is underlain by the softer soils. The site effects are most pronounced within Zone 2, in which the PGA exceeds 0.5 g at a number of locations. It is also noteworthy that the peak response is highly oscillatory across this region. Such rapid spatial variation of the ground motion has actually been observed in real earthquakes, e.g., during several aftershocks at clusters of sites that were instrumented in the aftermath of the 1994 Northridge earthquake (Hartzell *et al*, 1996; Bardet and Davis, 1996). This behavior can have important practical implications; yet, it is generally not possible to reproduce it via 1D simulations. To illustrate this point, and to help gain a better understanding of the differences between 1D and 2D effects on site response, a 1D simulation was also conducted for the idealized Kirovakan valley under consideration. For each mesh point on the valley surface a 1D analysis was performed for a soil column whose properties are identical to those beneath that point using as input the same incident SH-wave as for the 2D simulation. The distribution of the 1D PGA across the valley is also shown in Fig. 5b, by a dashed line. In contrast to the 2D simulations, the peak response is constant along sections where the valley bottom is flat, and varies only gradually as the valley depth changes, except near the edges. Overall, in Zone 2 the PGA is significantly greater for the 2D than for the 1D simulations.

In order to help explain the rapidly oscillatory nature of the PGA across the valley, it is convenient to filter temporarily the effect of the earthquake excitation and concentrate on the valley response to a simple steady-state harmonic excitation. The results are best observed in the frequency domain. Figure 6 shows the Fourier spectral ratio (FSR) of the response at site F near the point of maximum depth (shown in insert), as a function of frequency, corresponding to both the 2D and 1D simulations. This ratio is obtained by dividing the amplitude of the Fourier transform of the synthetic accelerogram at F by twice the amplitude of the Fourier transform of the free-field accelerogram (Fig. 4b). The two lines shown on Fig. 6 also represent the 1D and 2D amplification

ratios of the response at  $F$  with respect to the free-field motion on the surface of a halfspace made up of the same bedrock material as that underlying the valley model (Fig. 2), due to a steady-state harmonic vertically incident SH-wave. It is apparent from this figure that: (1) The 1D amplification ratio exhibits the resonant behavior typical of flat-layered systems. For this particular example the largest peak corresponds to the second resonance, in the vicinity of 2.5 Hz; (2) The 2D amplification ratio also exhibits resonant behavior in the vicinity of the 1D resonant frequencies, but the corresponding 2D frequencies are slightly higher than those for the 1D results, due to the lateral confinement of the valley. The values of the respective peaks, however, are considerably larger for the 2D case; (3) In addition to the essentially 1D resonant frequencies, the 2D valley experiences resonant behavior at other frequencies, which appear to be unrelated to the 1D case. The amplification ratio oscillates rapidly with frequency, reaching peak values that greatly exceed the 1D values. Interestingly, for certain frequencies the 2D amplification ratio is much smaller than unity, denoting, in effect, a strong deamplification, or destructive interference of seismic waves.

The Fourier spectral ratios shown in Fig. 6 are for a single point on the valley surface. To examine how the FSR varies from point to point, one can construct similar spectral curves for all the surface mesh points across the valley and plot the results as contour amplification ratios in terms of both frequency and location. These contours are shown on Fig. 7 for the 2D and 1D simulations, thus revealing simultaneously the spatial and frequency distribution of the ground motion. The scale of the FSR is given by the color bar. Similar contour displays have been presented by Sánchez-Sesma *et al* (1993) for homogeneous valleys of simple geometrical shapes. For the frequency range considered in Fig. 7, the 1D simulations exhibit four resonant frequencies near the deepest part of the softer subvalley. As expected, the values of these frequencies increase away from the center as the valley becomes shallower. Within the stiffer Zone 3 there is only one resonant frequency. The results of the 2D simulation are much more complex. First, multiple resonant frequencies occur throughout the valley. For some of these frequencies the amplification ratio reaches a maximum value of 8, almost double that for the 1D case. For each resonant frequency the amplification ratio exhibits several peaks, whose number increases with frequency. Between the peaks, the amplification ratio almost vanishes at certain locations. This means that the ground surface essentially remains at rest for these frequencies and locations, and experiences strong motion at nearby points. By contrast, for the 1D case the FSR varies only gradually across the valley.

To further elucidate these features of the response of the 2D valley, we consider next a simple example involving a rectangular, undamped, homogeneous valley of width  $L$ , depth  $H$ , supported on a rigid base and rigid side walls. While this model is substantially simpler than the valley under study, its dynamic behavior will prove to be useful for the interpretation of Fig. 7. Bard and

Bouchon (1985) have used the same example for a study that focused on the fundamental resonant response.

The natural frequencies of the valley, when subjected to antiplane vibrations, can be written as:

$$\frac{\omega_{mn}}{\omega_1} = \sqrt{(2m-1)^2 + n^2 \left(\frac{2H}{L}\right)^2}, \quad m, n = 1, 2, \dots \quad (5)$$

in which  $\omega_1$  is the fundamental natural frequency that the valley would exhibit if its width were infinite; i.e.,  $\omega_1$  is the natural frequency of a flat layer on a rigid base. Its value is given by  $\omega_1 = \pi V_s / (2H)$ , in which  $V_s$  is the shear wave velocity of the medium.

By setting the origin of a right-handed cartesian coordinate system at the lower left corner of the valley, the horizontal  $x$ -axis along the width, and the vertical  $y$ -axis toward the free surface, the mode shapes  $w_{mn}(x, y)$ , associated with the natural frequency  $\omega_{mn}$ , are given by:

$$w_{mn} = \sin \frac{(2m-1)\pi y}{2H} \sin \frac{n\pi x}{L}, \quad m, n = 1, 2, \dots \quad (6)$$

The integer  $m$  denotes mode shapes in the heightwise direction and  $n$  along the width. The first factor on the right side of Eq. 6 corresponds precisely to the mode shapes of the flat layer, whereas the second factor introduces the effect of the finite width. Thus, for each mode shape of the flat layer (i.e. for a fixed  $m$ ), there is a set of mode shapes in the widthwise direction with corresponding frequencies  $\omega_{mn}$ . Along the width the mode shape  $w_{mn}$  exhibits crests or troughs at a set of points  $P_{jn}$  with abscissas

$$x_{jn} = \frac{2j-1}{2n}L, \quad j = 1, 2, \dots, n, \quad n \geq 1 \quad (7)$$

while points  $Q_{jn}$  at

$$x_{jn} = \frac{j}{n}L, \quad j = 1, 2, \dots, n-1, \quad n \geq 2 \quad (8)$$

are nodes and remain at rest.

The locations of the points  $P_{jn}$  and  $Q_{jn}$  are shown on Fig. 8a together with their corresponding natural frequencies, for  $m = 1$  and a particular valley shape ratio ( $L/H = 3.1$ ). The corresponding points for  $m = 2$  (i.e. those associated with the second mode shape in the heightwise direction) are shown in Fig. 8b. The symbols, asterisks and circles, denote, respectively, extremum (crests and troughs) and nodal points. Thus, for instance, the mode shape  $w_{11}$  has a natural frequency  $\omega_{11} = 1.19\omega_1$ , a single extremum at  $x/L = 0.5$  and no nodes; the natural frequency associated with the mode shape  $w_{12}$ , which has two extremum values, at  $x/L = 0.25$  and  $0.75$ , and a nodal point at  $x/L = 0.5$ , is  $\omega_{12} = 1.69\omega_1$ ; similarly, the mode shapes  $w_{21}$  and  $w_{22}$  have natural frequencies  $\omega_{21} = 3.07\omega_1$  and  $\omega_{22} = 3.27\omega_1$ , and the same extremum and nodal points as  $w_{11}$  and  $w_{12}$ ; etc.

One can expect that if the valley is excited at a prescribed frequency  $\omega$ , those modes associated with the natural frequencies  $\omega_{mn}$  which are closest to  $\omega$  will be the ones that respond most strongly. The amplitude of the surface response will thus be greatest at points located near the critical points  $P_{mn}$  and smallest in the vicinity of the nodal points  $Q_{mn}$ .

The top plot in Fig. 7a shows that the idealized Kirovakan valley also tends to respond in its modal shapes, exhibiting crests and troughs, and nodal points, just like the much simpler rectangular valley, even though the Kirovakan model does not have separable mode shapes along its height and width. In fact, if one now examines the lines joining the extremum points and the nodal points, as shown in Fig. 8, the analogy between the two situations becomes apparent. We call the two sets of lines, extremum and nodal lines, respectively. From a comparison of Figs. 7 and 8, it is seen that the amplification ratio contours have a skeleton of extremum and nodal lines in the space-frequency domain and that the largest crests and troughs occur at distinct resonant frequencies akin to the natural frequencies of the simple rectangular valley. These resonant frequencies are given by the imaginary parts of the complex eigenvalues of the homogeneous problem associated with Eq. 2. The crests, troughs, and nodes are clustered along bands rather than lines, due to the presence of damping.

Notice that for the particular example of Kirovakan considered herein the larger amplification ratios do not correspond to the fundamental frequency, but occur at higher ones, with a clear 2D effect. It is also noteworthy that the motion in Zone 3 is influenced by that in Zone 2, by the energy that leaks through their interface; one can observe how the extremum and nodal lines generated within Zone 2 extend to Zone 3, although the amplitude of the response decreases drastically in the stiffer zone. None of these effects is present in the 1D simulation, as shown at the bottom plot of Fig. 7.

We return now to the earthquake problem in order to examine how the valley ground motion affects the response of structures located at different points within the valley. To this end, we consider next the pseudo-acceleration response spectra shown in Fig. 9a. In this figure, the maximum pseudo-acceleration  $A = (2\pi f_n)^2 u_{max}$ , in which  $u_{max}$  = maximum story drift of a single-story structure with an undamped natural frequency  $f_n$ . We recall that the maximum base shear,  $V$ , in the structure is related approximately to  $A$  through  $V/(mg) = A/g$ , in which  $m$  = mass of single-story structure. That is,  $A/g$  is the seismic coefficient by which the weight must be multiplied to obtain the maximum base shear. Jennings (1997) has shown that the base shear force of a regular  $n$ -story structure,  $V_{n-story}$ , can also be expressed approximately in terms of  $A/g$  for a single-story, as  $V_{n-story}/(Mg) = A/g$ , in which  $M$  is the total mass of the superstructure. Thus, the results of Fig. 9 can also be applied to regular multi-story buildings. The spectra in Fig. 9a were calculated for structures located at three different sites P, Q, R, identified in the insert, using as excitation

the synthetic accelerograms obtained at those points from the 1D and 2D simulations of the 1988 Armenia Earthquake. Soil-structure interaction is not taken into consideration. With an average shear wave velocity of 280 m/s over the top 30 m of soil in Zone 2, this effect is not expected to be significant for the structures and frequency range under study. Damping in the structures is 5 percent critical. Dashed and solid lines are used for the 1D and 2D results, respectively, and the suffix K in the key refers to Kirovakan. At points P (outside the valley) and Q (in Zone 3), the response spectra corresponding to the 1D and 2D simulations essentially coincide with each other. This indicates negligible 2D effects at these points. On the other hand, the 1D and 2D spectra for point R in the middle of Zone 2 show a huge discrepancy: the pseudo-acceleration for the 2D ground motion exceeds the corresponding results of the 1D simulation by as much as 100 percent. This clearly illustrates how 2D site effects can sometimes have a dramatic effect on the earthquake response of structures.

At this point it is of interest to compare the response spectra obtained for Zone 2 in Kirovakan with one derived for Leninakan, due to the very different levels of damage experienced in the two regions. The dashed-dotted line labeled L on Fig. 9a is the response spectrum calculated with a base excitation obtained from a 1D simulation using the soil properties for Leninakan reported by Yegian *et al* (1994b). The corresponding soil column was subjected to a vertically incident SH-wave with the reference rock motion scaled to 0.25 g, the estimated PGA at the rock outcrop in the Leninakan region. Since this city is located in a large and shallow valley, a 1D analysis seems sufficient for determining the soil amplification effects. Building-damage statistics indicate that 62 percent of the four- to five-story structures in Zone 2 in Kirovakan, with frequencies from 2.5 to 4 Hz, collapsed, whereas only 21 percent suffered the same fate in Leninakan. With this damage distribution one would expect that the response spectrum for Zone 2 should be significantly higher than the corresponding one for Leninakan. However, the computed spectra for L and R based on 1D ground motion simulations (Fig. 9a) are quite close to each other, especially for frequencies greater than 2.5 Hz. If, on the other hand, one compares the Leninakan spectrum with the solid line spectrum for R, corresponding to the 2D simulation in Kirovakan, it becomes clear that the seismic forces generated during the 1988 Armenia Earthquake must have been much stronger in Zone 2 in Kirovakan than in Leninakan. This is in agreement with the observed damage, and suggests that in order to explain the structural behavior within the Kirovakan Valley it is essential to take its finite lateral extent into consideration.

To gain further insight into the response of structures within Zones 2 and 3 in Kirovakan, the pseudo-acceleration spectra for several natural frequencies are shown in Figs. 9b to 9d for all points across the valley. These figures again illustrate that 2D site effects, in general, increase significantly the structural response over that from a 1D analysis. Moreover, the rapid spatial variation exhibited

by the ground motion amplification is also observed in the pseudo-acceleration spectra. This is of considerable practical importance, as it means that two identical structures separated by a short distance can be subjected to widely different seismic forces even if the underlying soils have essentially the same properties.

In order to examine simultaneously how the peak structural response caused by the valley ground motion varies with the structure's natural frequency and its location within the valley, a novel representation of the response in the form of space-frequency pseudo-acceleration spectra is introduced here. Results are presented in Fig. 10 for structures with 5 percent critical damping for the base excitations obtained from the 1D and 2D simulations. The natural frequency of the structure is given on the abscissa and the location within the valley is shown on the ordinate. The corresponding value of  $A/g$  is given by the color bar. Several observations can be made from this figure:

1. Structural response in Zone 3 is small compared to that in Zone 2. The strongest shaking occurs in the middle of Zone 2 and near its confluences with Zone 3 and the rock outcrop, for frequencies in the range of 2 to 5 Hz. These are precisely the locations within the valley and the natural frequency range for which damage was strongest during the 1988 earthquake.

2. The strongest response by far, however, corresponds to structures with natural frequencies close to 2.5 Hz. This is a classical double resonance phenomenon. Under the incident seismic wave, the valley responds in its most sensitive resonant mode shapes, whose frequencies almost happen to coincide with the dominant frequency (2.5 Hz) of the earthquake excitation (Fig. 4b). The second resonance occurs when the amplified ground motion produces strong vibration of structures whose natural frequencies coincide with those being excited in the soil deposits.

3. The 1D response spectra also predict resonant behavior near 2.5 Hz. The spectral ordinates, however, are much smaller than those for the 2D ground excitation. Also, whereas the 1D spectra are quite diffuse, the 2D spectra define sharp, localized regions, both in space and in frequency, for which the response is strongest. Overall, the spectral ordinates are significantly greater for the 2D case.

4. The 2D spectra exhibit islands of strong response in the 3 to 5 Hz region. The 1D spectra show no such behavior.

5. The nodal and extremum lines identified in the Fourier Soil Response Spectra in Fig. 7 are also apparent in the structural response spectra. While this response is largest within a region near the deepest portion of the valley, there is an adjoining region which essentially follows a nodal line. Thus, a small change in the structure's location can result in a dramatic change of its response. In addition, since the response spectra also vary rapidly with frequency, this means that two slightly

different structures located essentially at the same site can experience substantially different responses.

## CONCLUDING REMARKS

This study of the earthquake response of a small valley in Kirovakan during the 1988 Armenia Earthquake demonstrates how 2D ground motion simulations provide a suitable explanation of the observed damage in situations where 1D soil amplification analyses have proved to be unsatisfactory. The 2D simulations predict maximum ground and structural response in the frequency range of 2.5 to 4.5 Hz, which corresponds exactly to the natural frequencies of the four- to five-story structures which experienced the greatest damage. It appears that this damage occurred as a consequence of double resonance between the excitation, the valley, and the building structures. The amplitude of the double resonance was greatly enhanced by the finite lateral extent of the valley.

A novel way of visualizing structural response as a simultaneous function of the natural frequency of the structure and its location within the valley was introduced in this study. This allows one to identify the types of structures that are prone to suffer extensive damage and the locations within the valley where this damage is most likely to occur. In certain regions the soil and structural responses are seen to vary rapidly over short distances. This behavior, which has been observed during actual earthquakes, has practical implications for design.

In this study only one particular incident wave was considered. While thus restricted, results of this study suggest that simulations using realistic valley models could be used to great advantage in seismic zonation and seismic hazard analyses. Different earthquake scenarios consistent with the particular tectonic settings should, of course, be considered, and the simulation results integrated with those from observations. One might use a probabilistic approach to include effects from uncertainties in the source and model parameters.

## ACKNOWLEDGMENTS

Special thanks are given to Keiiti Aki, Francisco J. Sánchez-Sesma, and Yoshiaki Hisada for many useful discussions. Thanks also to M. K. Yegian for providing us the reference accelerogram for the 1988 Armenia Earthquake. This work was supported by the National Science Foundation's Grand Challenges in High Performance Computing and Communications program, under grant CMS-9318163. Funding comes from the Directorate for Computer and Information Science and Engineering, the Directorate for Engineering, and the Directorate for Earth and Atmospheric Sciences. In addition, NSF funding was supplemented with funds from the Advanced Research Projects Agency. The cognizant NSF program official is Clifford J. Astill. Computing services on the Pittsburgh Supercomputing Center's Cray T3D were provided under PSC grant BCS-960001P. We are grateful for this support.

## APPENDIX. REFERENCES

- Aki, K. and Larner, K. L. (1970). "Surface motion of a layered medium having an irregular interface due to incident plane SH-waves." *J. Geophys. Res.*, 75, 933–954.
- Aki, K. (1988). "Local site effects on ground motion." In Thun, J. L. V., editor, *Earthquake Engineering and Soil Dynamics II – Recent Advances in Ground Motion Evaluation*, pages 103–155, ASCE, New York.
- Aki, K. (1993). "Local site effects on weak and strong ground motion." *Tectonophysics*, 218, 93–111.
- Alterman, Z. S. and Karal, F. C. (1968). "Propagation of elastic waves in layered media by finite difference methods." *Bull. Seism. Soc. Am.*, 58, 367–398.
- Bao, H., Bielak, J., Ghattas, O., Kallivokas, L. F., O'Hallaron, D. R., Shewchuk, J., and Xu, J. (1996). "Earthquake ground motion modeling on parallel computers." In *Proc. 1996 ACM/IEEE Supercomputing Conference*, Pittsburgh, PA, November.
- Bard, P. Y. and Bouchon, M. (1980a). "The seismic response of sediment-filled valleys, part I. the case of incident SH waves." *Bull. Seism. Soc. Am.*, 70, 1263–1286.
- Bard, P. Y. and Bouchon, M. (1980b). "The seismic response of sediment-filled valleys, part II. the case of incident P-SV waves." *Bull. Seism. Soc. Am.*, 70, 1921–1941.
- Bard, P. Y. and Bouchon, M. (1985). "The two-dimensional resonance of sediment-filled valleys." *Bull. Seism. Soc. Am.*, 75, 519–541.
- Bardet, J. P. and Davis, C. (1996). "Engineering observations on ground motion at the Van Norman Complex after the 1994 Northridge earthquake." *Bull. Seism. Soc. Am.*, 86(1B), S333–S349.
- Bayliss, A. and Turkel, E. (1980). "Radiation boundary conditions for wave-like equations." *Comm. Pure Appl. Math*, 33, 707–725.
- Bielak, J. and Christiano, P. (1984). "On the effective seismic input for nonlinear soil-structure interaction systems." *Earthquake Engng. and Struct. Dyn.*, 12, 107–119.
- Bielak, J., MacCamy, R. C., McGhee, D. S., and Barry, A. (1991). "Unified symmetric BEM-FEM for site effects on ground motion—SH waves." *J. Engrg. Mech.*, 117, 2265–2285.



- Bommer, J. J. and Ambraseys, N. N. (1989). “The Spitak (Armenia, USSR) earthquake of 7 December 1988: a summary engineering seismology report.” *Earthquake Engrg. and Struct. Dyn.*, 18, 921–925.
- Boore, D. M., Larner, K. L., and Aki, K. (1971). “Comparison of two independent methods for the solution of wave-scattering problems: response of a sedimentary basin to vertically incident SH-waves.” *J. Geophys. Res.*, 76, 558–569.
- Boore, D. M. (1972). “Finite difference methods for seismic wave propagation in heterogeneous materials.” In Bolt, B. A., editor, *Methods in Computational Physics*, volume 11, Academic Press, New York.
- Borcherdt, R. (1989). “Results and data from seismologic and geologic studies following earthquake of December 7 1988, near Spitak, Armenia.” Technical Report No. 89-163A, USGS, Menlo Park, CA.
- Bouchon, M. and Aki, K. (1977). “Discrete wavenumber representation of seismic source wave-field.” *Bull. Seism. Soc. Am.*, 67, 259–277.
- Cisternas, A., *et al.* (1989). “The Spitak (Armenia) earthquake of 7 December 1988: field observations, seismology and tectonics.” *Nature*, 339, 675–679.
- Cremonini, M. G., Christiano, P., and Bielak, J. (1988). “Implementation of effective seismic input for soil-structure interaction systems.” *Earthquake Engrg. and Struct. Dyn.*, 16, 615–625.
- Foss, K. A. (1958). “Co-ordinates which uncouple the equations of motion of damped linear dynamic systems.” *J. Appl. Mech.*, 25, 361–364.
- Frankel, A. (1993). “Three-dimensional simulations of ground motions in the San Bernardino Valley, California, for hypothetical earthquakes on the San Andreas fault.” *Bull. Seism. Soc. Am.*, 83, 1020–1041.
- Hadjian, A. H. (1993). “The Spitak, Armenia earthquake of 7 December 1988 – why so much destruction.” *Soil Dyn. and Earthquake Engrg.*, 12, 1–24.
- Hartzell, S., Leeds, A., Frankel, A., and Michael, J. (1996). “Site response for urban Los Angeles using aftershocks of the Northridge earthquake.” *Bull. Seism. Soc. Am.*, 86(1B), S168–S192.
- Jennings, P. C. (1997). “Earthquake response of tall regular buildings.” Technical Report No. EERL 97-01, California Institute of Technology, Pasadena, California, January.

- Kallivokas, L. F., Bielak, J., and MacCamy, R. C. (1991). “Symmetric local absorbing boundaries in time and space.” *J. Engrg. Mech.*, 117, 2027–2048.
- Kawase, H. (1988). “Time-domain response of a semi-circular canyon for incident SV, P, and Rayleigh waves calculated by the discrete wavenumber boundary element method.” *Bull. Seism. Soc. Am.*, 78, 1415–1423.
- Lee, V. W. (1990). “Scattering of plane SH waves by a semi-parabolic cylindrical canyon in an elastic half-space.” *Int. J. Geophys.*, 100, 79–86.
- Li, X., Bielak, J., and Ghattas, O. (1992). “Three-dimensional earthquake response on a CM-2.” In *Proc. 10th World Conf. earthquake Eng.*, volume 2, pages 959–964, Madrid, Spain, Balkema, Rotterdam, The Netherlands.
- Lysmer, J. and Drake, L. A. (1971). “The propagation of Love waves across nonhorizontally layered structures.” *Bull. Seism. Soc. Am.*, 61, 1233–1252.
- Mossessian, T. and Dravinski, M. (1987). “Application of a hybrid method for scattering of P, SV, and Rayleigh waves by near-surface irregularities.” *Bull. Seism. Soc. Am.*, 77, 1784–1803.
- Sánchez-Sesma, F. J. and Esquivel, J. A. (1979). “Ground motion on alluvial valleys under incident plane SH waves.” *Bull. Seism. Soc. Am.*, 69, 1107–1120.
- Sánchez-Sesma, F. J., Ramos-Martínez, J., and Campillo, M. (1993). “An indirect boundary element method applied to simulate the seismic response of alluvial valleys for incident P, S and Rayleigh waves.” *Earthquake Engrg. and Struct. Dyn.*, 22, 279–295.
- Sánchez-Sesma, F. J. (1983). “Diffraction of elastic waves by three-dimensional surface irregularities.” *Bull. Seism. Soc. Am.*, 73, 1621–1636.
- Shewchuk, J. R. (1996). “Triangle: Engineering a 2D quality mesh generator and Delaunay triangulator.” In Lin, M. C. and Manocha, D., editors, *Applied Computational Geometry: Towards Geometric Engineering*, volume 1148 of *Lecture Notes in Computer Science*, pages 203–222, Springer-Verlag, May.
- Smith, W. D. (1975). “The application of finite element analysis to body wave propagation problems.” *J. Geophys.*, 44, 747–768.
- Spudich, P. and Iida, M. (1993). “The seismic coda, site effects, and scattering in alluvial basins studied using aftershocks of the 1986 North Palm Springs, California earthquake as source arrays.” *Bull. Seism. Soc. Am.*, 83, 1721–1724.

- Toshinawa, T. and Ohmachi, T. (1992). "Love wave propagation in a three-dimensional sedimentary basin." *Bull. Seism. Soc. Am.*, 82, 1661–1667.
- Trifunac, M. D. (1971). "Surface motion of a semi-cylindrical alluvial valley for incident plane SH waves." *Bull. Seism. Soc. Am.*, 61, 1755–1770.
- Vidale, J. E. and Helmberger, D. V. (1988). "Elastic finite-difference modeling of the 1971 San Fernando, California earthquake." *Bull. Seism. Soc. Am.*, 78, 122–141.
- Wong, H. L. and Trifunac, M. D. (74). "Surface motion of semi-elliptical alluvial valley for incident plane SH wave." *Bull. Seism. Soc. Am.*, 64, 1389–1408.
- Wyllie, L. J. and Filson, J. (1989). "Armenia earthquake reconnaissance report." *Earthquake Spectra*, Spec. Supplement.
- Yegian, M. K., Ghahraman, V. G., and Gazetas, G. (1994a). "1988 Armenia earthquake. I: seismological, geotechnical, and structural overview." *J. Geotechnical Engrg.*, 120, 1–20.
- Yegian, M. K., Ghahraman, V. G., and Gazetas, G. (1994b). "1988 Armenia earthquake. II: damage statistics versus geologic and soil profiles." *J. Geotechnical Engrg.*, 120, 21–45.
- Yegian, M. K., Ghahraman, V. G., and Gazetas, G. (1994c). "Ground motion and soil-response analyses for Leninakan, 1988 Armenia earthquake." *J. Geotechnical Engrg.*, 120, 330–348.
- Yegian, M. K., Ghahraman, V. G., and Gazetas, G. (1994d). "Seismological, soil and valley effects in Kirovakan, 1988 Armenia earthquake." *J. Geotechnical Engrg.*, 120, 349–365.

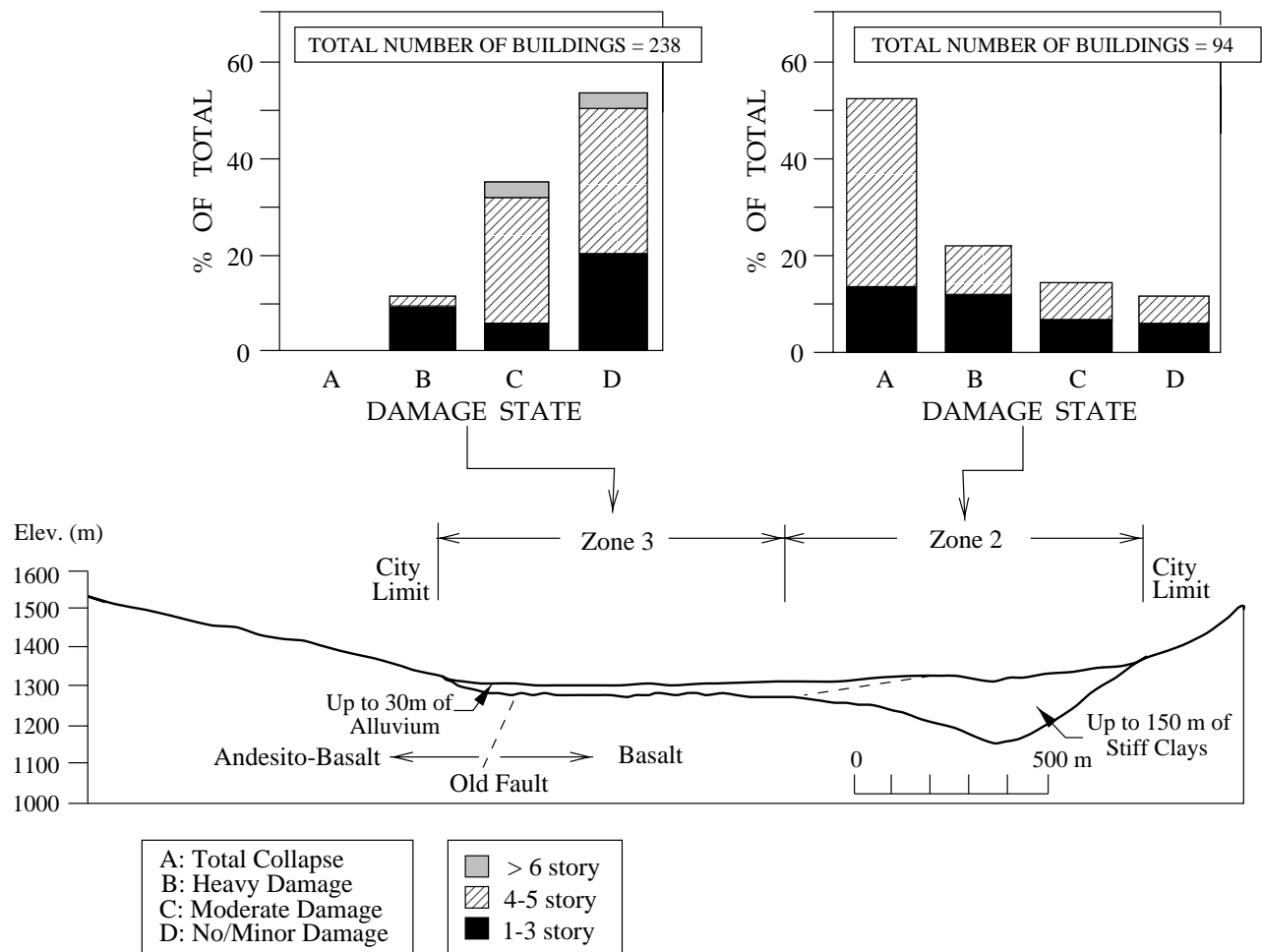


Figure 1: A geotechnical profile in Kirovakan and the corresponding damage statistics during 1988 Armenia earthquake (after Yegian *et al.*, 1994c).

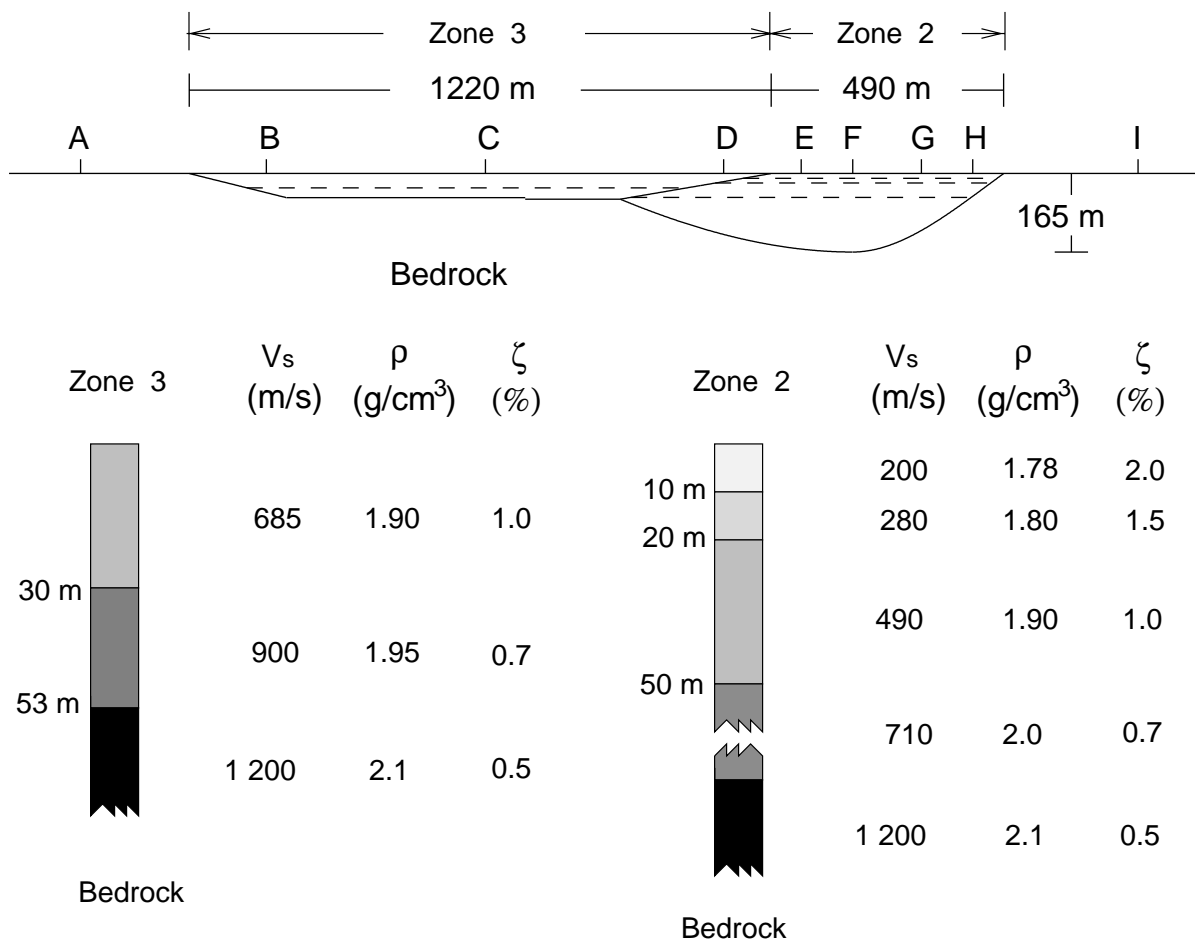
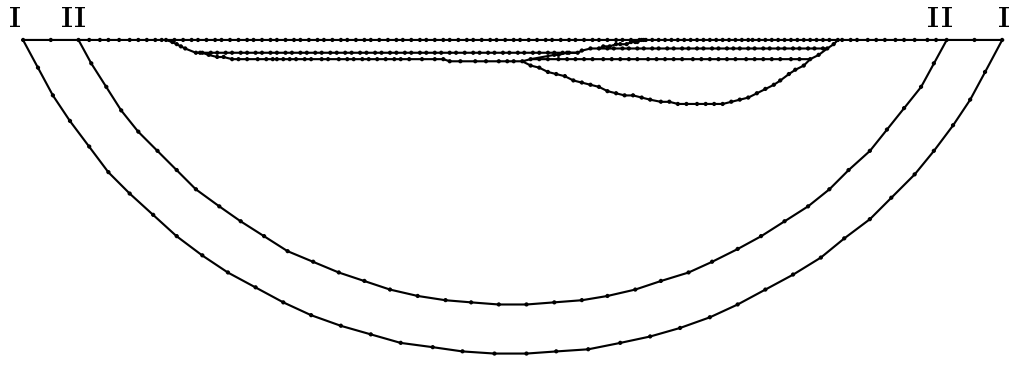
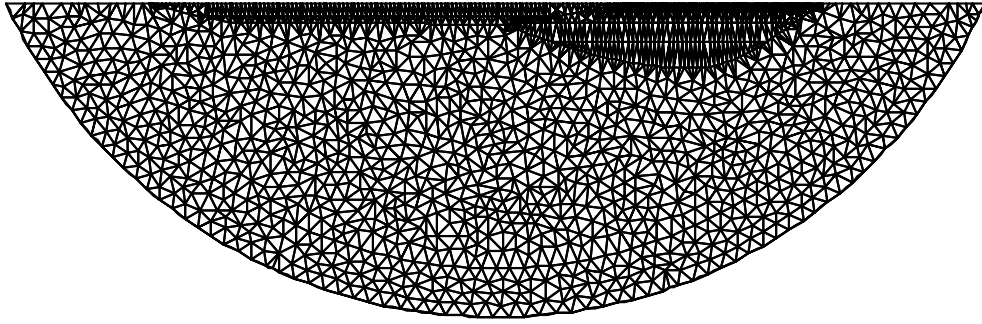


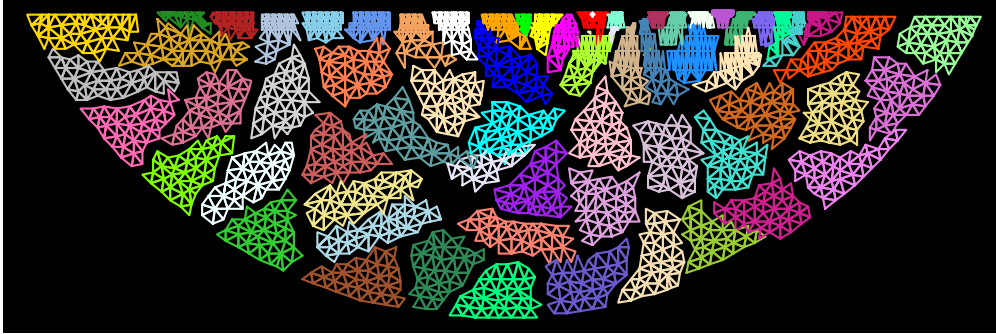
Figure 2: Geometry and material properties of the two-dimensional basin model.



(a)

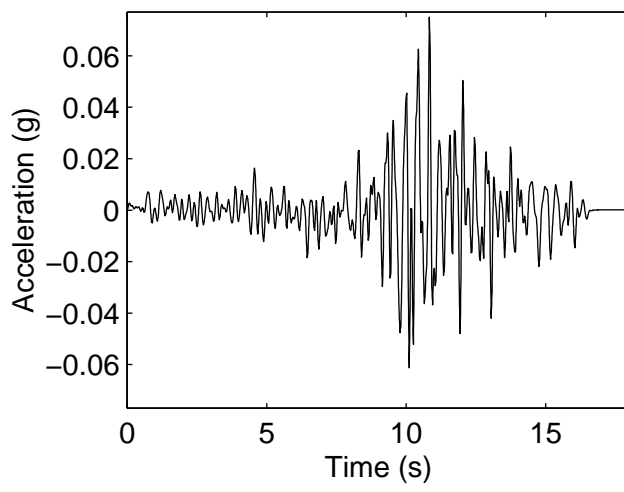


(b)

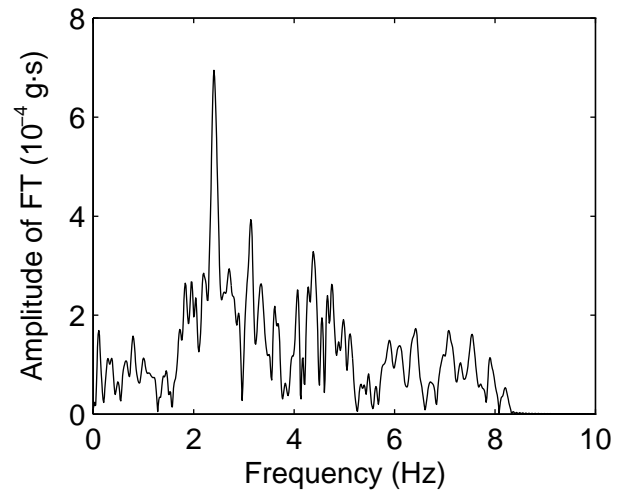


(c)

Figure 3: (a) Computational domain for the analysis of the basin model (top layer in Zone 2 not shown); absorbing boundary on I-I; effective forces applied on II-II; (b) Finite element mesh; (c) Partitioned mesh for parallel computing.

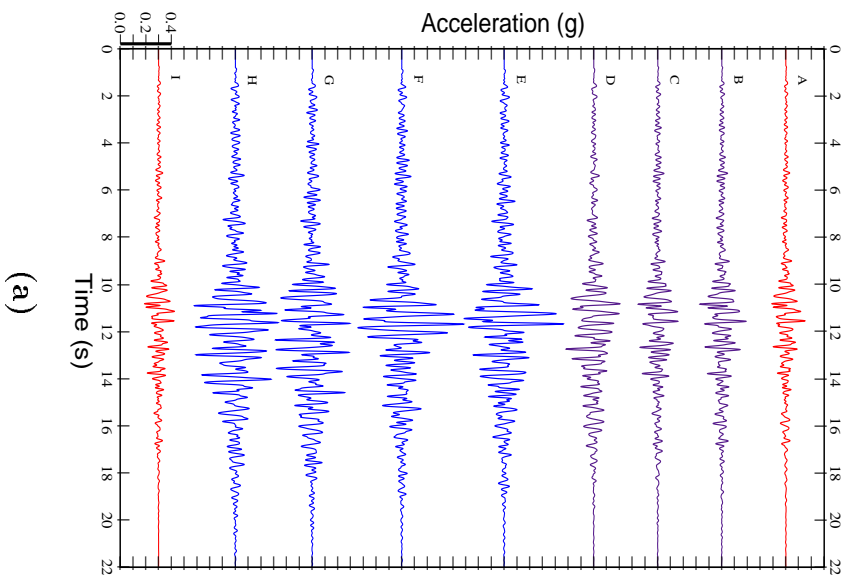


(a)

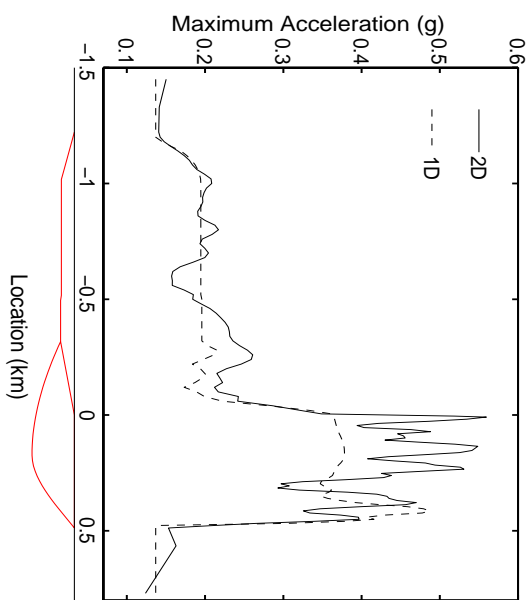


(b)

**Figure 4: (a) Scaled free field reference rock accelerogram for the incoming wave at depth for Kirovakan simulation; (b) Amplitude of its Fourier transform.**



(a)



(b)

Figure 5: (a) Synthetic accelerograms corresponding to 2D simulation of 1988 Armenia Earthquake for several surface points along the valley identified on Fig. 2; (b) Spatial variation of peak ground acceleration along the entire valley (corresponding to both 2D and 1D simulations).



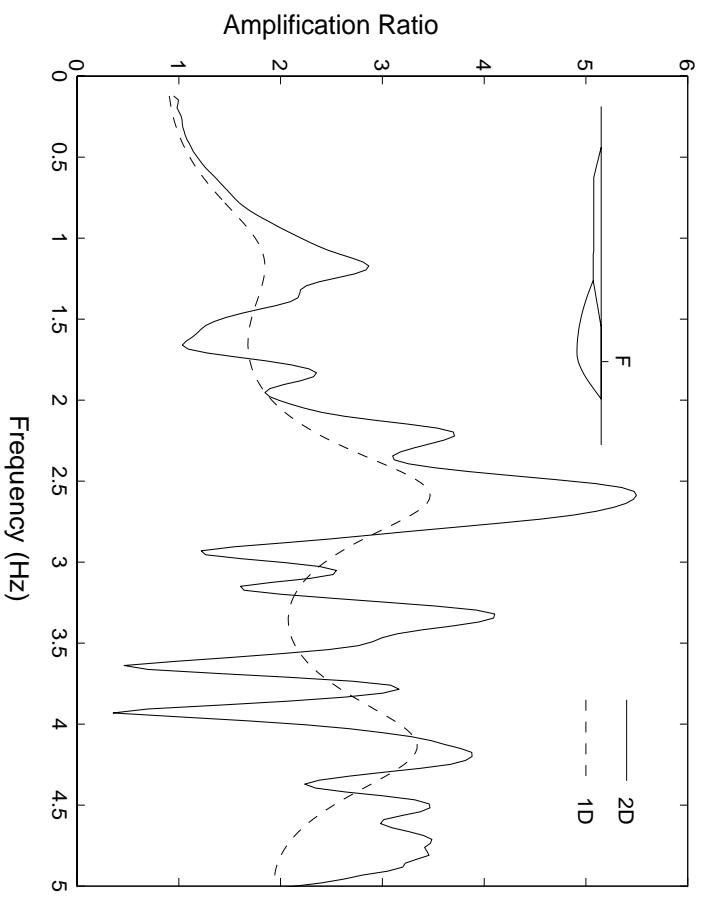


Figure 6: Fourier spectral ratio (FSR) at site F in Zone 2 (corresponding to both 2D and 1D simulations). Equivalently, normalized amplitude of the response at F due to a steady-state harmonic vertically incident wave.

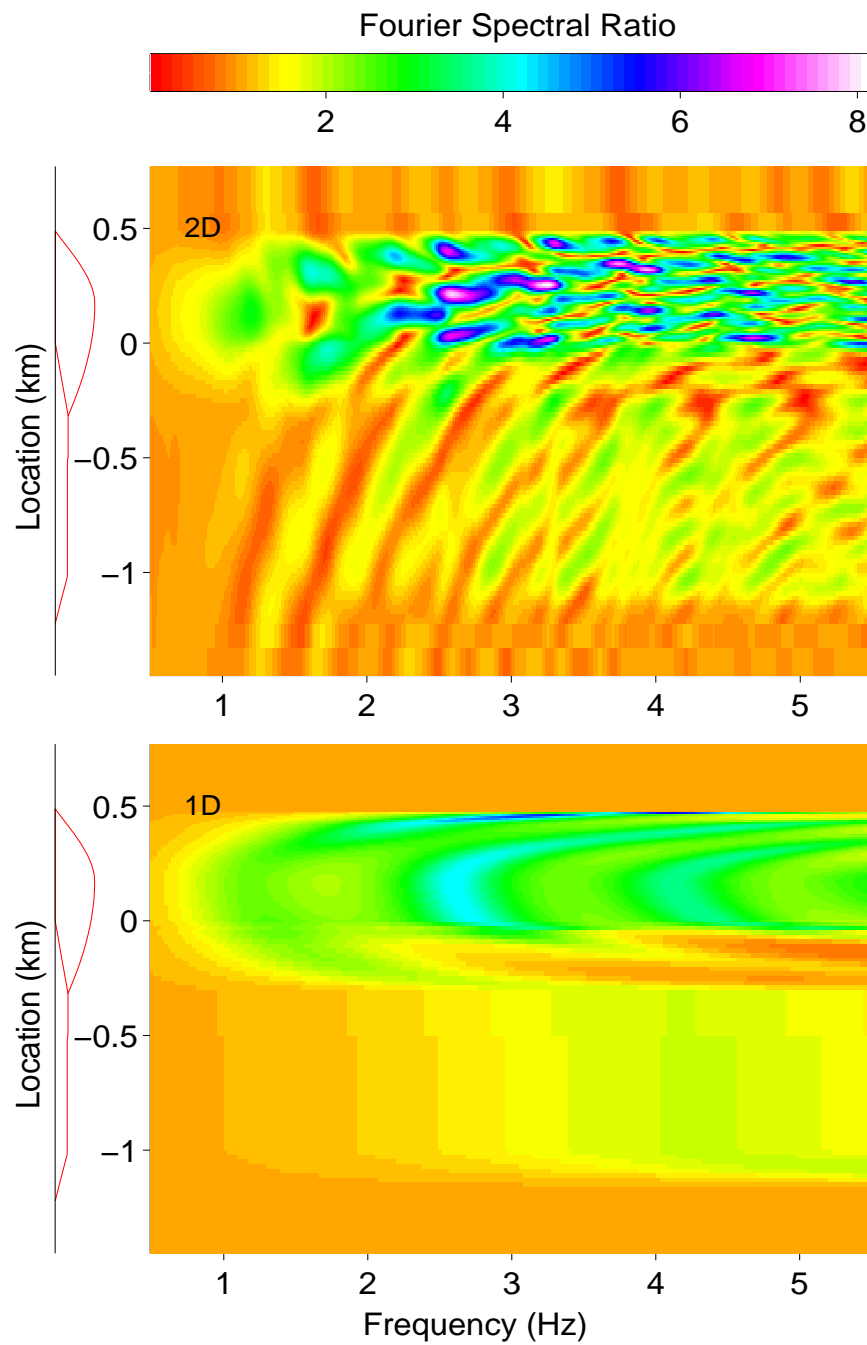
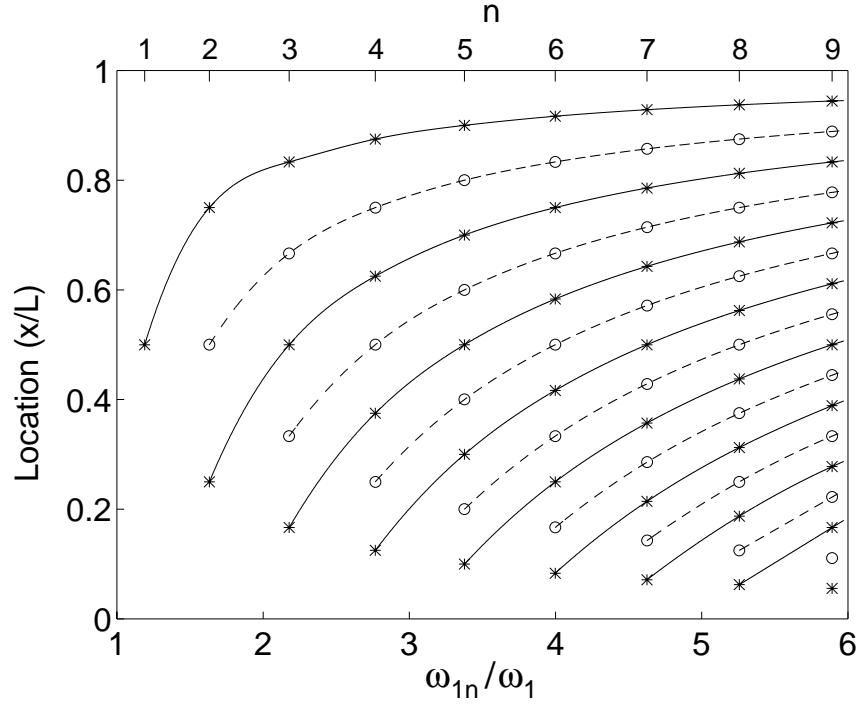
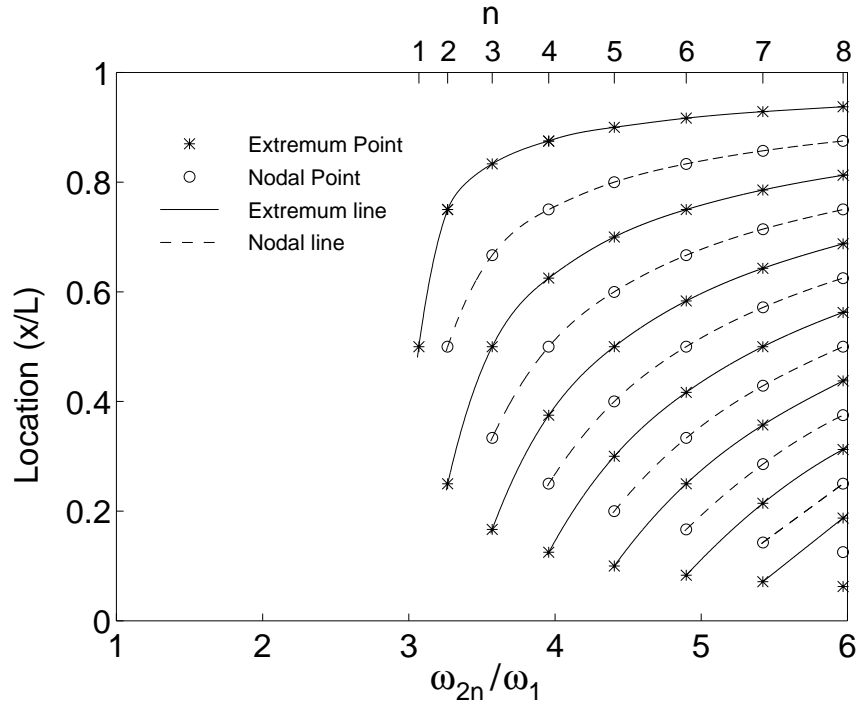


Figure 7: Fourier spectral ratio as a simultaneous function of position of observer and frequency. Top: 2D simulation; Bottom: 1D simulation.



(a)



(b)

Figure 8: Extremum and nodal points for several mode shapes  $w_{1n}$  and  $w_{2n}$ , and their corresponding frequencies  $\omega_{1n}$  and  $\omega_{2n}$ , for a homogeneous rectangular valley. These points are joined by the extremum line, and the nodal line, respectively.

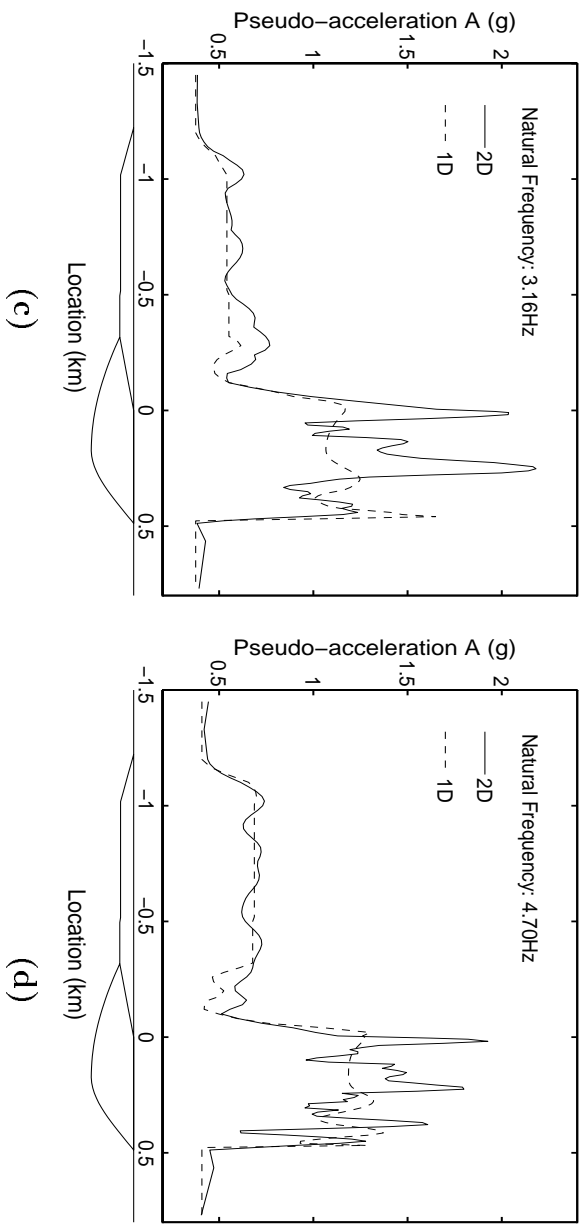
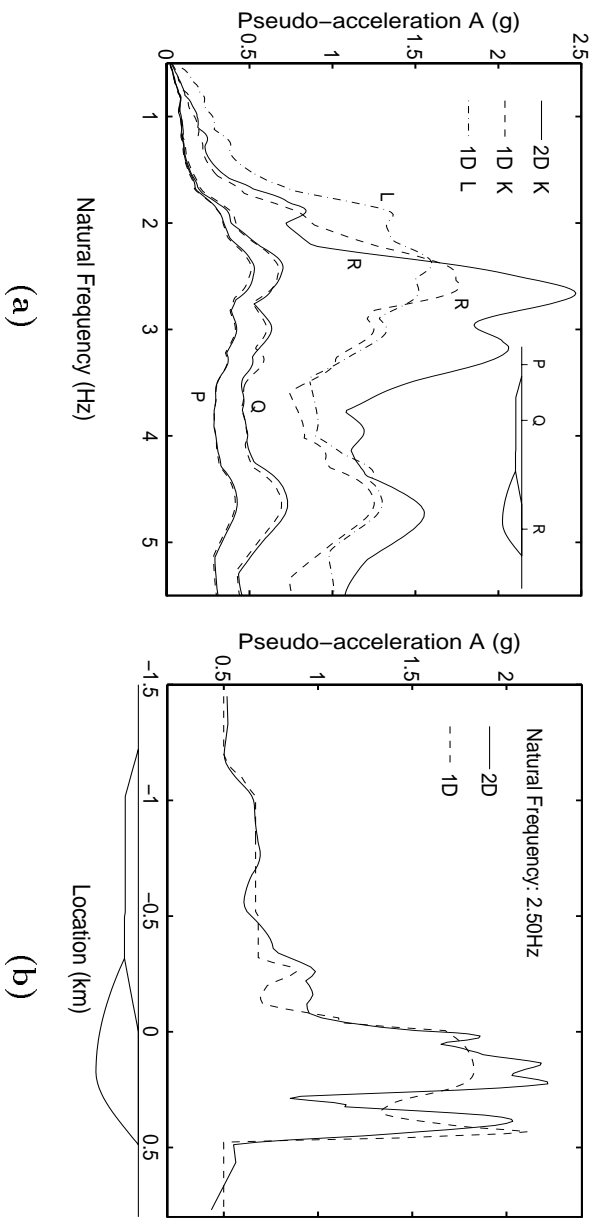


Figure 9: Pseudo-acceleration structural response spectra for five percent critical damping using ground motion synthetics from 1D and 2D simulations. (a) Response spectra for three sites in Kirovakan shown on insert and one in Leni-nakan, denoted by K and L, respectively; (b)–(d) Response along entire valley of Kirovakan, for three different natural frequencies.

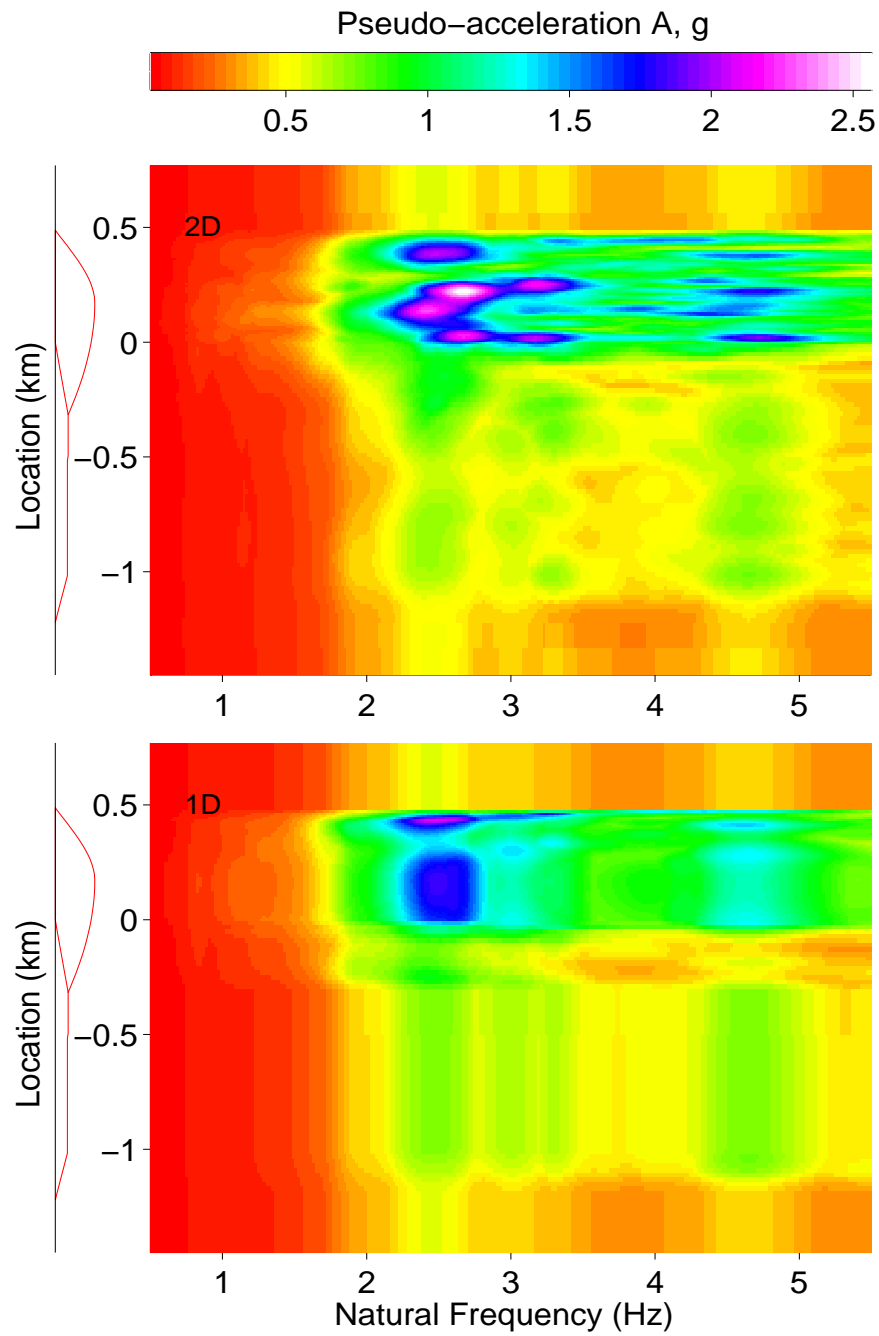


Figure 10: Pseudo-acceleration response spectra for five percent critical damping, as a simultaneous function of the location of the structure and its natural frequency. Top: For 2D simulation of 1988 Armenia Earthquake; Bottom: For corresponding 1D simulation.